oiling and Dryout in the PNC Local Blockage Experiments with 37-Pin Bundle

February, 1983

OARAI ENGINEERING CENTER
POWER REACTOR AND NUCLEAR FUEL DEVELOPMENT CORPORATION

PNC-TN941 83-15
Feb, 1983

10th Meeting of the Liquid Metal Boiling Working Group
(Oct. 27-29, 1982, Karlsruhe, Federal Republic of Germany)

BOILING AND DRYOUT IN THE PNC LOCAL BLOCKAGE EXPERIMENTS WITH 37-PIN BUNDLES

K. Yamaguchi and K. Haga

FBR Safety Engineering Division,
O-arai Engineering Center, Power Reactor and
Nuclear Fuel Development Corporation (OEC/PNC)
4002 Narita, O-arai, Ibaraki-ken, 311-13, Japan

ABSTRACT

Sodium boiling and dryout behavior behind planar blockages were examined with three 37-pin bundle experiments of different spacer and blockage type. Boiling inception within the grid spacer cells, closed on one side by the blockage, caused vigorous sodium boiling and subsequent dryout due to the restricted freedom of coolant movement. Local boiling behind the central blockage in the wire-wrapped pin bundle usually resulted in an oscillatory boiling pattern, while the transition to the stable boiling pattern was identified in one case. The edge blockage in the similar wire-wrapped bundle produced oscillatory or stable boiling patterns depending on the flow rates.

The difference and transition in the flow patterns were analyzed from the viewpoint of the volume balance of the vapor cavity to adjust the thermal and hydraulic boundary conditions at the two-phase interface region. The dryout data were intercompared to account for the location of the dryout position and the critical condition of the onset of local dryout. This study led to a model in which the liquid film on the pins within the vapor cavity varies in quantity mainly through the entrainment generation and the deposition of the entrained droplets.

NOMENCLATURE

A	:	flow area
D_B	:	characteristic length of the blockage
d	:	pin diameter
d_h	:	equivalent diameter of the flow area
E_b	:	imaginary deposition rate of entrained droplets to compensate for the lack of deposition rate under the presence of counter current film evaporation
E_d	:	deposition rate of entrained droplets in the absence of film evaporation
E_e	:	entrainment generation rate
E_v	:	evaporation rate of liquid film
F	:	fraction of blocked flow area

G_e : total mass flow rate of entrainment
G_f : total mass flow rate of liquid film
G_o : total mass flow rate of coolant
P : pressure at the heated section
p : pin pitch
q" : heat flux
T : temperature
T^* : hypothetical temperature in the absence of boiling
ΔT_{ms} : theoretical excess temperature, $T^* - T_{sat}$
ΔT_{sub} : subcooled temperature (degree of subcooling), $T_{sat} - T$
t : time
U_o : inlet velocity
U_B : velocity at the blocked plane, $U_o/(1 - F)$
x : quality
z : axial distance from the blockage

Subscripts
core : core flow region (outside blockage)
max : maximum
cr : critical (dryout)
sat : saturation
sub : subcooling
IB : inception of boiling

INTRODUCTION

A local blockage within a fuel subassembly of a Liquid Metal Fast Breeder Reactor (LMFBR) results in both a local cooling disturbance within the wake and a global flow reduction in the subassembly. In certain cases, these two consequences have sufficient potential to raise sodium temperatures in the wake to saturation, and cause local boiling (1).

The principal issue concerned with the local boiling experiments is to examine the possibility of fuel failure propagation. This study requires knowledge of the effect of boiling upon flow and heat transfer stability, and of the coolability margin beyond which the localized dryout and cladding melting occur behind the initially assumed blockage. Pin bundles of different types have been used for similar tests in several laboratories. These include the grid spacer type full bundle test sections with central and corner blockages at Kernforschungszentrum Karlsruhe (KfK) (2),(3),(4),(5), the triangular pin bundles simulating a 1/6 sector of grid spacer type full bundles with equivalent central blockage at Energieonderzoek Centrum Nederland (ECN) (6),(7),(8), and the grid or wire spacer type intermediate hexagonal pin bundles with central and edge blockages at Power Reactor and Nuclear Fuel Development Corporation (PNC) (9),(10). The differences in the bundle geometries complicate the understanding of local boiling and dryout, because the geometrical configuration of the test bundle is a very sensitive parameter to boiling behavior.

The present paper is addressed to the intercomparison of these experimental results. Emphasis lies in the discussions concerning the derivation of a general heat transfer model in a trapped vapor cavity behind the blockage, and the transition from one flow pattern to another and its effect on the boiling crisis. Our interests are focused here on three PNC experiments conducted with 37-pin bundles having different spacers and blockages.

EXPERIMENTAL METHOD

SIENA Facility

The local boiling tests were conducted with the Sodium Boiling and Fuel Failure Propagation Test Facility, SIENA, in the O-arai Engineering Center (OEC/PNC). Figure 1 shows the schematic diagram of the loop. It has a main pump, expansion tank, separator tank, air cooler, auxiliary heater, and other miscellaneous components to form a conventional sodium loop. The cold-leg sodium temperatures were sustained around 750 K, with the oxygen content being kept below 10 ppm and the cover gas pressure about 0.10 MPa.

The tested bundles are installed in turn on the attachment ports of the T-3 test section. The other two paths from the main pump to an expansion tank can be used for bypass flow. Part of the sodium driven by the main pump enters the test section, flows up through the pin bundle where it is heated to cause local boiling. Since the voided region is restricted within the narrow region downstream from the blockage, the single-phase hot sodium leaves the test section toward the expansion tank, where it mixes with the bypassed sodium, and moves to a subsequent separator tank. After leaving these tanks, the sodium enthaply is lowered by an air cooler to maintain the cold-leg sodium temperature constant.

37-Pin Bundles

In order to simulate different conditions in an LMFBR fuel subassembly, four different 37-pin bundles were fabricated. However, the grid spacer type edge-blocked bundle named 37GE was not used for the boiling experiments due to its early pin trouble. The detailed specifications of the test bundles are shown in Figs. 2 and 3, and Table 1. All pin bundles used dummy pins in the unblocked region so as to easily sustain the desired subcooling in the core flow region during each local boiling run.

The diameter of each pin was 6.5 mm and the pin pitch was 7.9 mm. The axial heated length of the heater pin was about 460 mm and the heat flux was uniform. Grid spacers of 15 mm height were located with an axial pitch of 200 mm for the first two 37-pin bundles (37GC and 37GE), while a spacer wire of 1.3 mm diameter was wrapped around each pin with a helical pitch of 265 mm for the last two 37-pin bundles (37WC and 37WE). Near the middle position of the heated section, a stainless steel blockage of 5 mm thickness was attached. For the 37GC and 37GE bundles, the blockages closed the upstream end of the grid spacers. The blockages (and grid spacer walls) covered 39, 58, 26 and 50 % of the total flow areas, respectively.

Instrumentation

Pin surface temperatures were measured by 0.3 mm diameter thermocouples embedded into pin cladding. The same diameter thermocouples were immersed in the subchannel centers for sodium temperature measurement. Some of the spacer wires of 1.3 mm diameter served as the thermocouples. All thermocouples were calibrated prior to the experiments by checking their outputs at some typical isothermal condition with nearly the same sodium temperature as the inlet sodium temperature for the test. The inlet sodium flow rate and pressure were measured by an electromagnetic flow-meter and a pressure transducer, both attached on the inlet piping. The inlet flow velocity was calculated by multiplying the reading of the flow-meter by the conversion factor predetermined to satisfy the heat balance through the test section.

These signals were processed by a digital data acquisition and reproduction system.

Operating Procedure and Experimental Condition

The operating procedure of the local boiling runs was as follows: A steady-state single-phase condition was first attained. Then, the pin power was increased stepwise to raise the power-to-flow ratio. Before and after local boiling was monitored, the pin power of each step was held steady long enough to confirm that the new flow patterns were stationary. In case a dryout experiment was projected at the beginning of a run, the pin power was increased until a sudden interruption of the power supply to the heater pins, which was initially programmed to act when dryout was sensed by the thermocouples, terminated the run automatically.

The range of the operating conditions attained during the local boiling runs is summarized in Table 2, and the detailed experimental conditions of the last steps of all dryout runs are rearranged in Table 3. A total of four runs provided the dryout data.

EXPERIMENTAL RESULTS

Dryout at the Grid Spacer Plane

Figure 4 shows the signal history of the dryout run conducted with the grid spacer type 37GC bundle. Dryout followed immediately after boiling inception at the restricted region surrounded by the grid spacer walls. All signals drawn in Fig. 4 reveal drastic changes of heat transfer during the short period of about 10 seconds. The sodium vapor "explosion" characterized by the onset of a sodium density wave was identified by the oscillations of pressure and flow signals. Also identified was the long existence of a vapor cavity, since no pressure spike pulse was observed until power trip, indicating that there was no collapsing of the vapor cavity.

Not only during the initial single-phase steps but also during the subsequent boiling and dryout steps, individual sodium and cladding surface temperatures behave with quite distinctive manners relative to neighboring thermocouple locations. These characteristics can be ascribed to the disconnected behavior of stagnant sodium within the laticed hexagonal cells. The grid spacer was designed to permit free sodium streaming through concave walls with vertically cut lines. However, the lateral sodium flow through these windows looks insufficient to wash out the vapor cavity from the cell. The local pressure gradient which causes reverse flow within the wake would also depress the buoyancy movement of the vapor cavity.

The overlap of these events led to the cladding melting of five pins illustrated in Fig. 4. However, neither the vapor "explosion" nor the cladding melting induced any significant flow excursion. Therefore, it may be concluded, concerning the local fault accident scenario, that the coolability condition will become similar to that in the bare bundle having a planar blockage, once the cladding within the grid spacer is melted together with the inner grid walls. This situation coincides with the results of the studies at KfK and ECN.

Dryout in the Wire-Wrapped Bundle with Central Blockage

Local boiling behind the central blockage in the wire-wrapped pin bundle, 37WC, usually resulted in an oscillatory boiling pattern. Figure 5 shows the result of the dryout run (9), where the oscillatory boiling pattern governs the phenomena in almost all the time period of these boiling steps. During one cycle of the oscillations, sodium temperatures change at most by 30 K around their mean values. The inlet flow-meter signal revealed that the frequency of the oscillations was around 10 Hz, which decreased slightly with

increasing power-to-flow ratio.

Permanent dryout appeared at the fifth step of power increase after the boiling inception step, i.e. at the step when the power-to-flow ratio was raised up to 131 % of the initial value at the boiling inception step. Prior to the dryout, the hydraulic oscillation damped gradually into a stabilized state. The stabilization in this case was not the result of forming a steady thermal balance between the vapor cavity and the surrounding core flow, but a slow axial expansion of the vapor cavity trying to attain a new effectively cooled condition. However, a stable vapor cavity was not reached before local pin failure appeared.

The isotherms of sodium and boiling boundaries for every step are illustrated in Fig. 6, where the mean values of sodium temperatures are used to draw the isotherms. It is seen from Fig. 6 that the void volume and the isotherms of the surrounding liquid phase swell slightly in the radial direction throughout the power steps while keeping their characteristic shapes almost constant. However, no axial expansion of the voided region was identified except for the final stage, although the vapor cavities at the later steps should have been noticeably larger than the ones actually observed, if the cavity volume were specified solely by the power-to-flow mismatch ratio with respect to the boiling inception condition. This fact reveals that a single vapor cavity may be trapped within the depressurized zone behind the blockage; there still exists a pressure field similar to that of single-phase flow, where the axial extent of the wake region is about 55 mm.

A permanent dryout first appeared on the pin surface facing the first subchannel at the plane 22 mm downstream from the blockage. This position had been near the upper and lateral ends of the boiling region throughout the oscillatory boiling period. During the slow and large axial expansion of the vapor cavity, the dryout region expanded radially toward the second subchannel at the same plane and axially toward the blockage at the first subchannel. The experiment was automatically terminated at this stage. Therefore, whether the vapor cavity attains a new steady balance or returns to the oscillatory pattern again, yet with a slow frequency and large volume change mode, is not known from this experiment. The possibility of the flow excursion which causes subsequent failure propagation apparently does not exist for both cases.

Dryout in the Wire-Wrapped Bundle with Edge Blockage

Figures 7 and 8 show two dryout runs of different type observed in the edge blockage wire-wrapped pin bundle, 37WE[1]. The histories of the isotherms during these runs are illustrated in Figs. 9 and 10, respectively, where the time of each frame is arbitrarily chosen.

For this bundle configuration, the wake length of the single-phase flow is about 100 mm. The temperature field in the low flow velocity (U_B = 3.62 m/s) run is, in general, not so steep with respect to the distance from the wake center as that observed in the high flow velocity (U_B = 5.46 m/s) run. This is mainly due to the contribution of the molecular heat conduction, which is effective in the low flow run. Therefore, the boiling region at the immediate instance of boiling inception in the low flow run (Fig. 9(a)) is located around the reattachment point of the wake contour on the wapper tube surface, where the sodium flow stagnates with large fluctuations and the heat conducted from the hot wake center is added to yield the secondary hot region. As the flow velocity increases, the heat transport is controlled by convection alone.

1 Note that the data in Fig. 7 may give a misleading interpretation due to the inevitable humming between the plotting frequency and the observed oscillatory boiling frequency.

Then, the temperature field becomes wavy. This situation causes different boiling onset points as is obviously shown in Fig. 10(b), where the local boiling starts within the wake region and expands by a great amount until the thermal and hydraulic equilibrium is achieved[2]. As will be discussed later, the saturation isotherm must satisfy an extra boundary condition, viz, it is a constant pressure surface, by adjusting the surrounding flow field. The high flow run, which causes a larger pressure gradient during the single-phase condition than that in the low flow run, requires a large amount of adjustment at the instance of boiling inception. This adjustment can be read from Figs. 10(a) through (c).

When the power is raised enough to form a single developed vapor cavity, the oscillatory boiling is induced in the low flow run, while the boiling pattern in the corresponding high flow run is still stable. The boiling boundaries of both runs exceed the initial wake reigons of the early single-phase steps. Only during the high flow run there are equilibrium states which permit the vapor cavity to stay quiescent while satisfying the steady pressure balance at its surface. Dryout was suddenly reached at a power step 16 % higher than that of the boiling inception step. On the other hand, the boiling region of the low flow run extended more widely than that which could be predicted from the result of the high flow run, and was more effectively cooled by the oscillations upto about 30 % higher power, while some parts of the pin surfaces repeated dryout and rewetting during each cycle of the oscillations.

DISCUSSION

Transition of Boiling Patterns

Similar experiments were conducted at KfK (3),(4),(5) and ECN (6),(7),(8). All runs with central or equivalent blockages showed oscillatory boiling patterns irrespective of absolute pressure levels and pressure gradients along the boiling regions. On the other hand, the corner blockage experiments at KfK showed both oscillatory and stable boiling patterns (3),(5). These findings are consistent with those of the 37WC and 37WE experiments at PNC. In addition, the KfK test results also suggested that the dryout condition should be examined separately depending on whether or not the local boiling is stable.

Although KfK used a 169-pin bundle with a 21 % corner blockage, the current results are helpful in estimating the stability condition of the vapor cavity generated behind the ~20 % edge blockage in a 169-pin bundle, i.e. the thermohydraulic equivalent condition of the 37WE bundle. All data available are correlated in Fig. 11 to show the operating parameter region of stable boiling, where the subcooled temperature and the core flow velocity were chosen as axes of the map, because these two were key parameters of the heat removal in single-phase flow (11) and a similar heat transfer mechanism as the heat exchange layer model for the single-phase flow was thought effective in the present case. Some unstable boiling data do not necessarily culminate in permanent dryout but never change to a stable pattern even if the pin power is raised enough to cause permanent dryout.

There is a distinct difference, at least, in the flow velocity regions of the PNC and KfK runs in which the boiling patterns are stable. KfK's five

2 From the temperature and pressure signals shown in Fig. 8, we can guess that faint and temporary boiling might have occurred at lower pin power steps ($q'' = 154$ and 160 W/cm^2) than the one corresponding to the obviously identified boiling step ($q'' = 167$ W/cm^2) shown in Fig. 10(b).

dryout runs with middle flow velocities (U_B = 2.5 to 4 m/s) and one with high flow velocity (U_B = ~ 5 m/s) showed stable boiling patterns, and the seven runs with low flow velocities (U_B < ~ 2.5 m/s) and three with high flow velocities terminated under oscillatory boiling patterns. Clare (3) claims that the extra convective cooling introduced by the oscillatory motion of a cavity in a high flow run leads to lower mean temperatures in the wake and to a smaller mean cavity volume than the one which would be expected in steady boiling (as was the case in the 37WC experiment at PNC). This interpretation indicates that KfK's unstable vapor cavities at the high flow runs seem to require larger cavity volumes in order to be balanced thermodynamically in the fields of low subcooling (ΔT_{sub} = ~ 350 K). The vapor cavity at the high flow run with high subcooling (ΔT_{sub} = ~ 500 K), on the contrary, attained adequate (small) volume for its stabilization in the steep pressure gradient field. Moreover, the vapor cavities at the middle flow runs with low subcooling also attained sufficient (large) volumes in the mild pressure gradient fields.

On the other hand, the volume of unstable vapor cavity observed in the PNC low flow run was too large from the standpoint of thermodynamic balance. This over-extended cavity formation may be ascribed to the mild pressure gradient field, because the vapor cavity was stable with smaller volume in the case when the pressure gradient field was steep. Consequently, it is concluded that the relation between the cavity volume needed for stabilization and the amount of pressure gradient along the boiling region is equal both for PNC's data and KfK's data; viz, the steeper the pressure gradient is, the smaller is the stable cavity volume. A similar conclusion can be drawn for the subcooling; the higher the subcooling is, the smaller is the stable cavity volume. The important point is whether or not these two are satisfied at the same time. This equilibrium condition was found to be satisfied in PNC's geometrical configuration only at the high flow region, and was satisfied in KfK's geometrical configuration at the middle flow region and high flow region with highly subcooled temperatures.

Vapor cavities cannot stay quiescent in the very low flow velocity situations due to their superior buoyancy. Even without these buoyancy forces, the vapor cavity would be unstable in the low flow velocity case, because the pressure field loses its ability to restrict the vapor cavity within a small volume which balances with the heating condition. The cavity volume in such a case will be, therefore, larger than the one which would be expected in steady boiling, as was the case in the PNC low flow velocity run with the 37WE bundle.

Based on the above facts, we can construct the following picture of the equilibration process of the cavity volume to adjust the thermal and hydraulic boundary conditions at the two-phase interface region. It is illustrated in Fig. 12, where the temperature field was extrapolated from the data shown in Figs. 6, 9 and 10, and the pressure field was estimated from the backdata of the water mockup test shown in Fig. 13 (12). For a given stable cavity volume, there are definite quantities of the cavity surface heat current and the cavity surface constant (saturation) pressure profile. Furthermore, there is another relation to be satisfied between these two quantities: the cavity surface heat current must be removed by the surrounding coolant whose coolability depends on the conduction and convection performance, i.e. the washout intensity of the sodium stream. Otherwise, the cavity surface behaves as a "moving boundary." The constant pressure profile at the cavity surface requires, from the hydrodynamic needs, another appropriate sodium flow streaming which directly gives feedback to the cooling condition. When the cavity volume is changed with the change of operating power or flow rate, for instance, the sodium stream lines should be adjusted to satisfy a new relation among all quantities

mentioned above. If the adjustment leads to an equilibrium state, the boiling pattern is sustained or becomes stable; otherwise it will have failed in its oscillatory pattern to satisfy the equilibrium condition on average.

On the basis of this hypothesis, one can understand why the boiling pattern is geometry dependent, since the geometry defines the possible temperature and pressure fields. The vapor cavity behind any central blockage will have a smaller stable boiling region compared with that behind an edge or corner blockage. This is mainly due to the difference in the ratios of the cavity volume to the surface: A little expansion of the central cavity introduces a drastic change of the total amount of heat removal, while the same volume expansion of the edge or corner cavity, on the contrary, would produce a small change. It is clear, however, that if the hypothesis is correct, the precise prediction of the boiling pattern in a differently blocked bundle with a particular operating condition will depend on the capability to calculate the temperature and pressure fields precisely. A conventional steady state calculation which separately treats the relations between many quantities mentioned before will give the rough scope on this point, but the detailed solution has not been found thus far[3].

Structure of the Vapor Cavity

In all dryout runs, permanent dryouts were detected near the upper and lateral ends of the boiling boundaries. Dryout was also identified near the laterally centered position of the blocked section neighboring the planar blockage. Figures 6, 9 and 10 reveal that these points are located commonly at slightly inside the boiling boundaries, where the vapor condensation appears most pronounced, since the temperature fluctuations at these points are extremely large in comparison with those measured at the other boiling boundary points. The temporary dryout was found within the wide region when the boiling pattern was oscillatory. Despite our intuitive viewpoint, the center of the temporary dryout region shows rather good coolability.

Figure 14 shows a picture on the quality distribution which will give a clear grasp of these situations. The vapor is generated within the cavity region through the evaporation of liquid film on the pin surfaces. The pin surfaces which are located near the boiling boundary can be easily filled with sodium. The liquid entry, however, is insufficient for the pins standing always within the vapor cavity. Therefore, the liquid films on the surface of these inner pins should be supplied mainly by the deposition of the entrained droplets. The amount of the entrainment increases at the subchannels facing richly flooded pins because of the shedding effect of the liquid film at the instant of violent evaporation and the mechanical shearing-off effect of the wavy liquid film by the passing vapor jet, whose velocity in the cavity is believed to reach the order of 100 m/s (3),(6). From the isotherm data, the most entrainment-rich region appears to be situated at the axially central position.

On the vapor condensation surface, the vapor cavity is depressurized. The depressurization produces a pressure gradient within the cavity and then the rush of subsequent vapor and entrainment mixture is directed upward or downward depending on the pressure gradient. During the rush, the net amount of entrained droplets decreases gradually due to the deposition and the succeeding

3 If the subcooling of the core flow were too low (temperature too high) to drive the conflicting condensing behavior against the expanding vapor cavity, the flow excursion might result. However, such a condition is not the scope of the present study but of the Core Disruptive Accident (CDA) study.

evaporation. The mass transfer gradually reduced decreases the thickness of the liquid film and the amount of entrainment, and, therefore, increases vapor quality until the liquid film vanishes completely. This situation leads to the following general formulation of the dryout quality in the forced convection system:

$$x_{cr} = 1 - G_e/G_o \quad , \tag{1}$$

where the mass flow rate balance of the liquid film and the entrainment at the instance of dryout is:

$$\frac{dG_f}{dz} = - A\,(E_e - E_d + E_b + E_v) = 0 \quad , \tag{2}$$

$$\frac{dG_e}{dz} = A\,(E_e - E_d + E_b) \quad , \tag{3}$$

where E_v is the film evaporation rate which is given by dividing the heat input by the latent heat; E_d is the deposition rate in the absence of evaporation which will be controlled by the turbulent diffusion of the droplets; and E_b is the imaginary deposition rate of entrained droplets to compensate for the lack of the deposition rate under the presence of evaporated vapor flow countering against the droplet-free diffusion direction. The precise formulations of each term in Eqs. (2) and (3) are beyond our scope, while the physical model of the vapor and droplet mixture flow within the cavity leads to a consistent interpretation of the location of each dryout point.

The oscillatory boiling is, from the hydraulic standpoint, a turbulence promotor which intensifies repetitively the source term of the entrainment generation. This causes the rewetting of the dried pin surfaces through the abrupt increase of the droplet deposition. The central region of the cavity with high entrainment is, therefore, relieved from early pin melting.

Instead of evaluating x_{cr} directly, a tentative approach to correlate the dryout heat flux in terms of the theoretical excess temperature, $\Delta T_{ms} = T^*_{max} - T_{sat}$, was tried by Dorr and de Vries (7), where T^*_{max} is the hypothetical peak temperature in the absence of boiling. The theoretical excess temperature is a scale of the boiling intensity and is related to the amount of heat that is transfered from the boiling zone to the surrounding liquid flow through evaporation and condensation of the coolant. The theoretial excess temperature is not known from experiment. Instead, it is calculated in the present paper by multiplying the reference peak temperature rise at the instance of boiling inception by the increased fraction of power-to-flow ratio at a dryout condition:

$$T^*_{max} - T_{core} = \Delta T_{sub} \frac{(q''/U_B)_{cr} - (q''/U_B)_{IB}}{(q''/U_B)_{IB}} \tag{4}$$

The calculated results of $\Delta T_{ms,cr}$ for the stable boiling dryout data available are shown in Table 4. The results for the KfK data indicate that the ΔT_{ms} seems to attain a constant critical value ($\Delta T_{ms,cr} = 208 \pm 20$ K) at the instance of parmanent dryout, although at present we cannot identify the effects of q''_{cr}, ΔT_{sub}, U_B and other possible parameters on the critical ΔT_{ms}. The hypothesis of a constant critical ΔT_{ms} means that the constant x_{cr}

criterion might hold for the disturbed bundle geometries, indicating the appropriateness of the cavity structure model shown in Fig. 14. Then, the corresponding dryout criterion for the PNC bundle configuration becomes $\Delta T_{ms,cr}$ = 74 K ± 10 %. The difference between the critical ΔT_{ms} values obtained at PNC and KfK can be regarded as being caused by the differences in subchannel flow area and spacer type.

CONCLUSIONS

Four cases of dryout runs were conducted with three different types of 37-pin bundles with blockages. The results were summarized referring to the similar test results by others and the following conclusions have been drawn concerning the boiling crisis.

(1) Three different types of dryout phenomena were observed: Boiling inception within the grid spacer cells, closed on one side by the blockage, caused vigorous sodium boiling and subsequent dryout due to the restricted freedom of the coolant movement. Local boiling behind the central blockage in the wire-wrapped pin bundle usually resulted in an oscillatory boiling pattern, while the transition to the stable boiling pattern was identified in one case. The edge blockage in the similar wire-wrapped bundle produced both oscillatory and stable boiling patterns depending on the flow rates.

(2) The operating parameter region of stable and unstable boiling was identified to yield a stability map whose axes are subcooled temperature and flow velocity. It enabled us to provide the intepretations of the individual test results with consistent phenomenological understanding of the transition mechanism of boiling patterns.

(3) A heat transport model of the coolant within the vapor cavity was identified as entrainment-controlled, and this successfully accounted for the location of the dryout position and the critical condition of the onset of local dryout. This model indicated the possible approach of correlating the dryout data observed in various blockage configurations in terms of the constant critical excess temperature.

For the local fault assessment, an extrapolation of the present knowledge to a general blockage case must be conducted. It will be treated in the future study (1).

ACKNOWLEDGMENTS

The authors are indebted to Drs. Y. Kikuchi, Y. Daigo, and Messrs. K. Sahashi, M. Uotani, T. Isozaki and T. Komaba for their engineering and technical contributions throughout the performance of individual experiments. The authors particularly wish to express their thanks to Dr. C. L. Larson and Miss T. Ohtsu for their efforts on manuscript preparation.

REFERENCES

(1) Yamaguchi, K., Nakamura, H., and Haga, K., "Boiling and Dryout Conditions in Disturbed Cluster Geometry and Their Application to the LMFBR Local Fault Assessment," to be presented at the Second International Topical Meeting on Nuclear Reactor Thermalhydraulics, Santa Barbara, California, Jan. 1983.

(2) Huber, F., and Peppler, W., "Form and Development of Boiling behind a 49% Central Blockage in a 169 Pin Bundle," Proceedings of the 7th Liquid Metal Boiling Working Group Meeting, Petten, June 1977.
(3) Clare, A. J., and Huber, F., "Boiling and Dryout in the KNS Local Blockage Experiments," Proceedings of the 9th Liquid Metal Boiling Working Group Meeting, Rome, June 1980.
(4) Huber, F., and Roberts, D., "An Evaluation of the Boiling Oscillations Observed in the 49 % Central KNS Local Blockage Experiment," Proceedings of the 7th Liquid Metal Boiling Working Group Meeting, Petten, June 1977.
(5) Clare, A. J., "Pin Cooling and Dryout in Steady Local Boiling," KfK-2944, Apr. 1980.
(6) Dorr, B., de Vries, J. E., and Maarleveld, J. R. C., "Sodium Boiling and Pin Dryout behind Plane Flow Blockages (The ECN/KfK Local Boiling Experiments)," Proceedings of the 9th Liquid Metal Boiling Working Group Meeting, Rome, June 1980.
(7) Dorr, B., and de Vries, J. E., "The ECN/KfK Local Boiling Experiments in Petten," Proceedings of the 8th Liquid Metal Boiling Working Group Meeting, Mol, Oct. 1978.
(8) de Vries, J. E., Hoebe, J. C., and Dorr, B., "Local Boiling in a Test Bundle Simulating a Sixth Part of a LMFBR Subassembly Having a Large Flat Type Central Flow Blockage," ECN-77-137, Sep. 1977.
(9) Yamaguchi, K. et al., "Local Temperature Rise and Boiling Behavior behind a Central Blockage in a Wire-Wrapped Pin Bundle," Proceedings of the 9th Liquid Metal Boiling Working Group Meeting, Rome, June 1980.
(10) Uotani, M., and Haga, K., "Local Sodium Boiling Experiments in Simulated LMFBR Fuel Subassemblies," Proceedings of the International Meeting on Liquid Metal Fast Breeder Reactor Safety and Related Design and Operational Aspects, Lyon, July 1982.
(11) Yamaguchi, K. et al., "Experimental Investigation of Local Cooling Disturbances in LMFBR Fuel Subassembly, ASME Winter Annual Meeting, 81-WA/HT-40, 1981.
(12) Nakamura, H., Miyaguchi, K., and Takahashi, J., "Hydraulic Simulation of Local Blockage in a LMFBR Fuel Subassembly," Nuclear Engineering and Design, Vol. 62, Dec. 1980, pp. 323-333.

Table 1 Summary of the pin bundle geometries

Pin bundle		37GC†	37GE†	37WC†	37WE†	MONJU
Pins (Heaters)**		37 (19)	37 (22)	37 (19)	37 (22)	169 -
Heated section length	(mm)	456	459	455	455	930
Blockage location††	(mm)	304	308	300	255	-
Blockage thickness	(mm)	5	5	5	5	-
Wrapper tube width	(mm)	50.4	50.4	50.4	50.4	104.6
Wrapper tube thickness	(mm)	10	10	10	10	3
Pin diameter	(mm)	6.5	6.5	6.5	6.5	6.5
Pin pitch	(mm)	7.9	7.9	7.9	7.9	7.87
Flow area	(mm^2)	915.5	915.5	924.3	924.3	3636.1
d_h	(mm)	3.51	3.51	3.43	3.43	3.22
D_B	(mm)	29.4	25.2	29.4	25.2	-
F	(-)	0.39*	0.58*	0.26	0.50	-
Spacer wire diameter	(mm)	-	-	1.3	1.3	1.32
Axial pitch of spacers	(mm)	200	200	265	265	307

* This value includes the area occupied by the grid spacer walls.
** These values mean the numbers of actually heated pins during runs.
† GC = grid spacer, central blockage; GE = grid spacer, edge blockage; WE = wire spacer, central blockage; WE = wire spacer, edge blockage.
†† Distance from the bottom of heated section to the downstream end of blockage.

Table 2 Operating parameter ranges sustained during the local boiling experiments with 37-pin bundles

Pin bundle	U_o (m/s)		q" (W/cm^2)		T_{in} (K)		T_{sat} (K)	
	min.	max.	min.	max.	min.	max.	min.	max.
37GC	0.30	3.51	65.1	237.4	717	787	1181	1189
37WC	0.89	2.73	90.0	192.0	692	764	1173	1188
37WE	0.86	3.11	67.4	237.4	686	761	1178	1199

Table 3 Experimental conditions of the dryout runs

Pin bundle	Run No.	U_B (m/s)	q" (W/cm^2)	T_{in} (K)	P (MPa)	T_{sat} (K)	Boiling pattern at dryout	$\frac{q"_{cr}-q"_{IB}}{q"_{IB}}$
37GC	37(19)GLB-101	1.5	68	736	0.133	1189	expansion	0
37WC	37(19)WLB-114	2.4	167	764	0.130	1187	oscillatory -> stable	0.31
37WE	37(19)WEB-142	3.62	164 167	742	0.135	1185	oscillatory	0.28 0.30
	37(18)WEB-143	5.46	194	738	0.145	1195	stable	0.16 (0.26)

Table 4 Summary of the dryout runs conducted with ~ 20 % edge blockage bundle or equivalent

	Bundle	Blockage	$q"_{cr}$ (W/cm^2)	U_B (m/s)	ΔT_{sub} (K)	T_{sat} (K)	$\frac{q"_{cr}-q"_{IB}}{q"_{IB}}$ (%)	Critical ΔT_{ms} (K)
PNC	37-pin	50 % edge	194.0	5.46	457	1195	16.2 (26.0)	74 (119)
KfK	169-pin*	21 % corner	165.0 106.8 128.1 135.0 79.1 97.0	5.06 3.84 3.82 3.80 2.56 2.54	509 350 434 505 344 427	1203	36.9 64.8 52.1 42.0 60.4 52.3	188 227 226 212 208 223

* d_h = 6.4 mm, d = 6.0 mm, p = 7.9 mm, grid spacer type

Note:
The values in the parentheses of Tables 3 and 4 were tentatively obtained using q" = 154 W/cm^2 as a boiling inception heat flux.

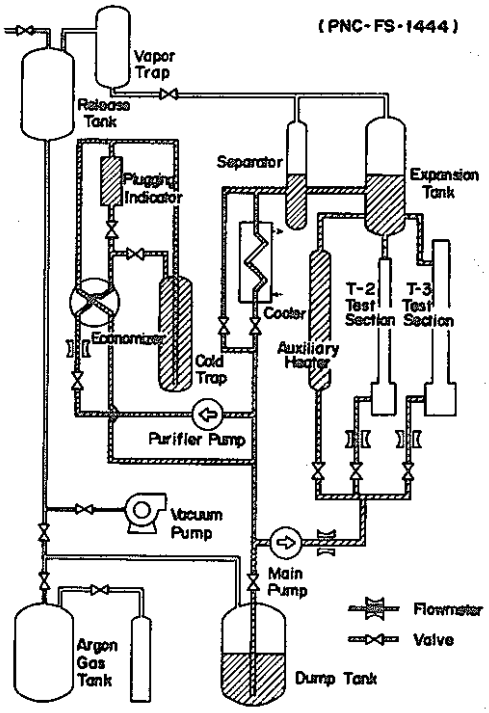

Fig. 1 Schematic diagram of Sodium Boiling and Fuel Failure Propagation Test facility, SIENA

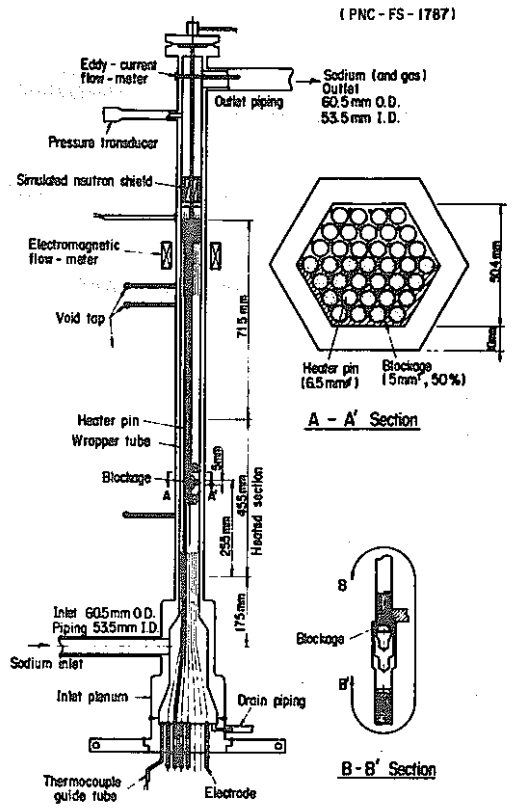

Fig. 2 Wire-wrapped 37-pin test bundle with edge blockage (37WE)

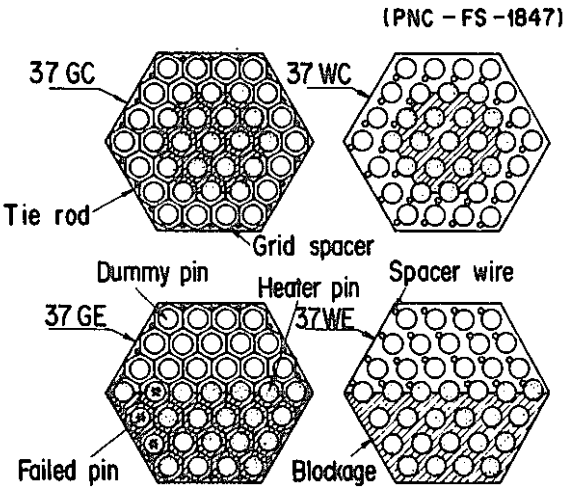

Fig. 3 Cross sections of 37-pin bundles having different spacers and blockages

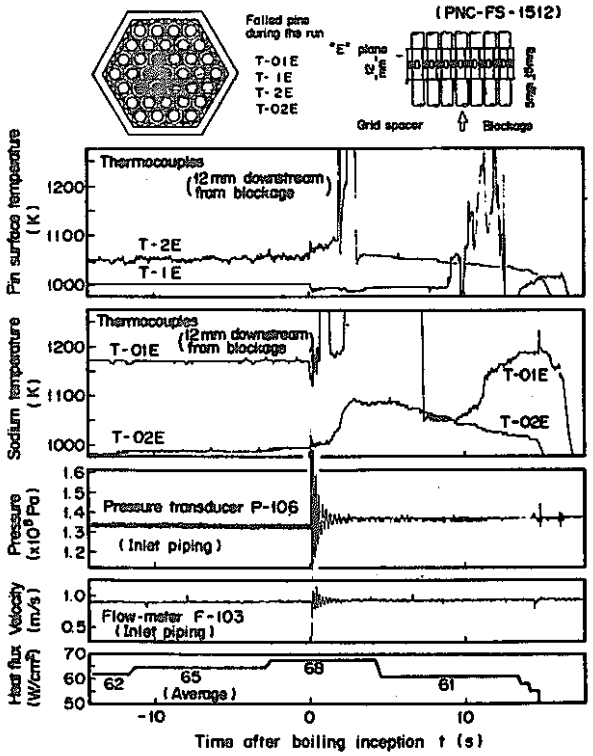

Fig. 4 Signals of temperatures, inlet pressure, flow velocity and heat flux during dryout run 37(19)GLB-101

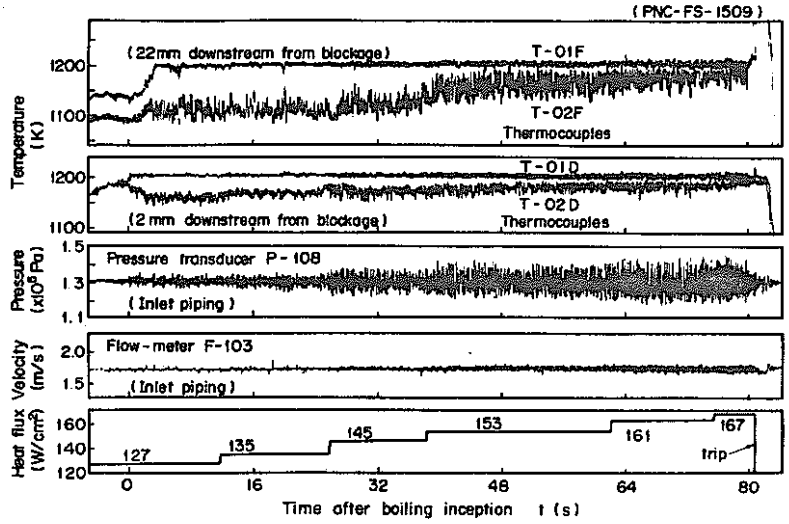

Fig. 5
Signals of sodium temperatures, inlet pressure, flow velocity and heat flux during dryout run 37(19)WLB-114

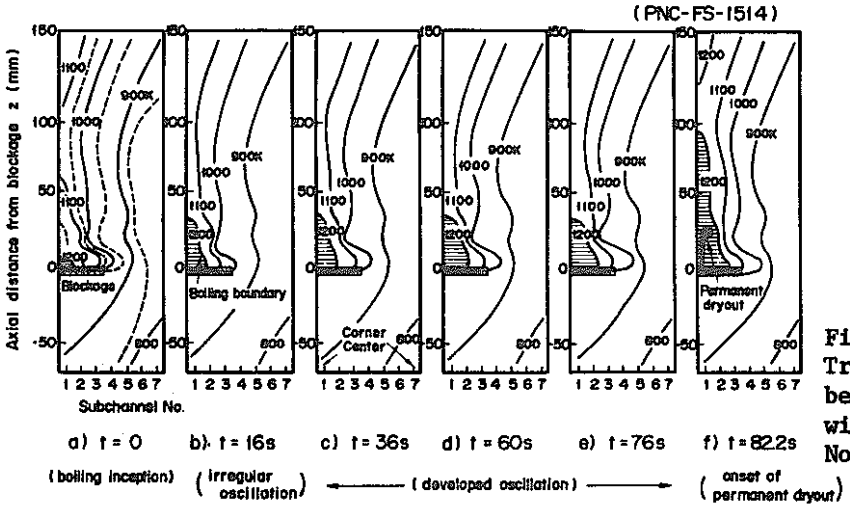

Fig. 6
Transition of the isotherms behind the central blockage of wire-wrapped 37-pin bundle (Run No. 37(19)WLB-114)

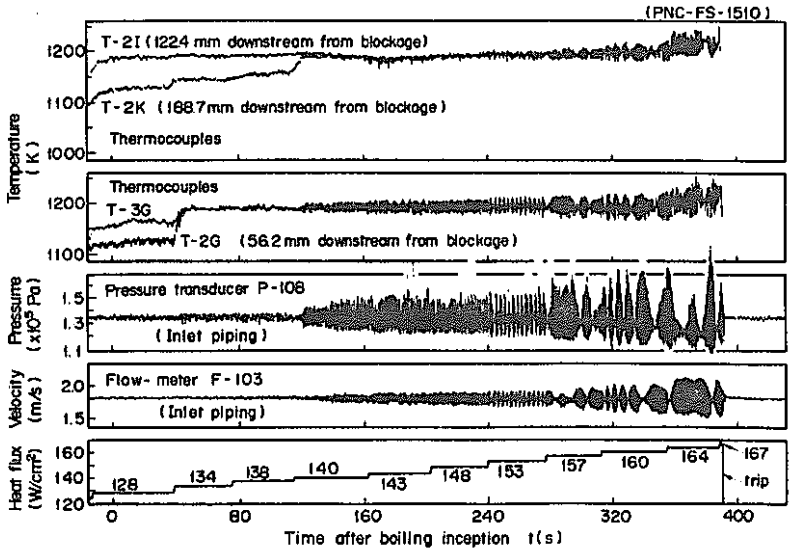

Fig. 7
Signals of sodium temperatures, inlet pressure, flow velocity and heat flux during dryout run 37(19)WEB-142

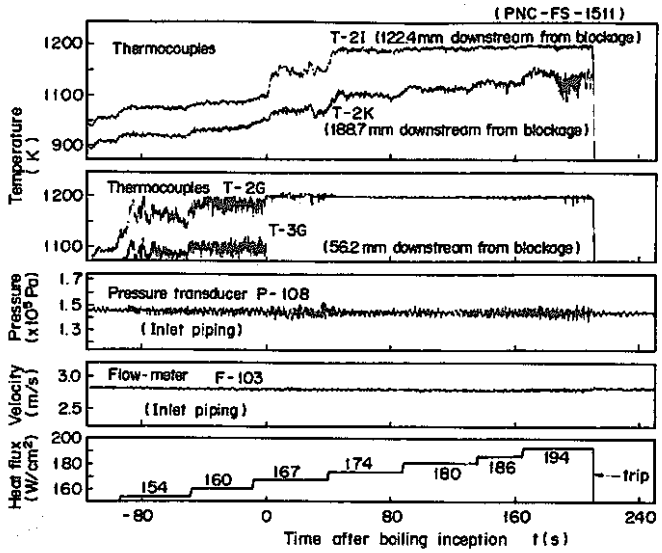

Fig. 8 Signals of sodium temperatures, inlet pressure, flow velocity and heat flux during dryout run 37(18)WEB-143

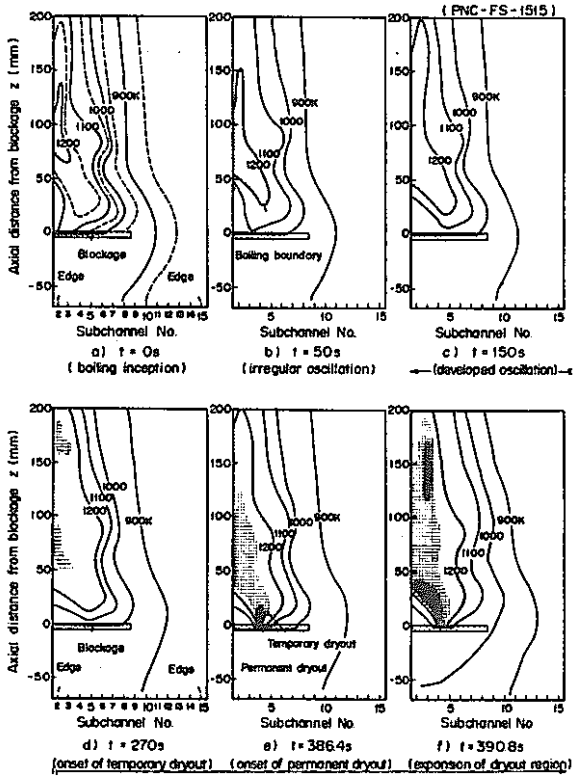

Fig. 9 Transition of the isotherms behind the edge blockage of wire-wrapped 37-pin bundle (Run No. 37(19)WEB-142)

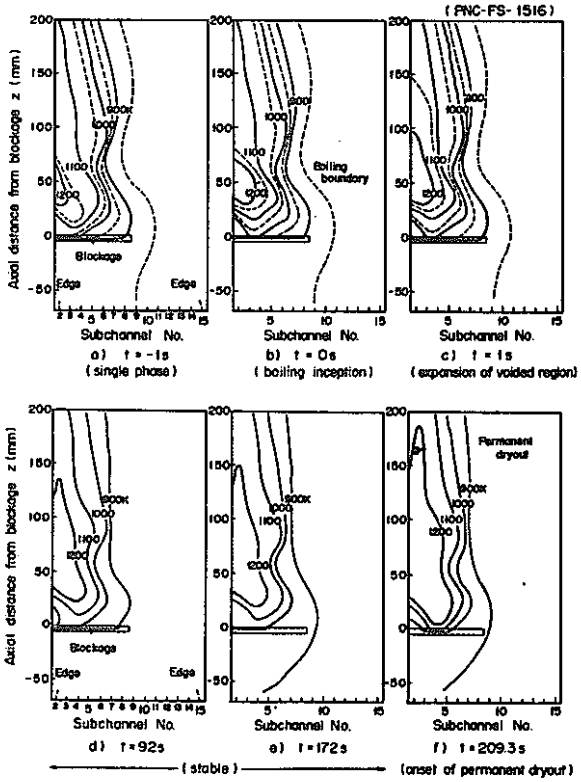

Fig. 10 Transition of the isotherms behind the edge blockage of wire-wrapped 37-pin bundle (Run No. 37(18)WEB-143)

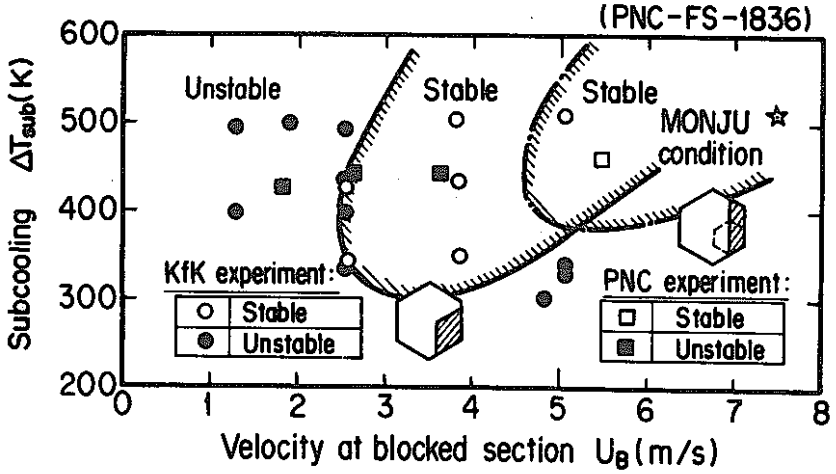

Fig. 11 Correlation of the local boiling pattern in the cases of ~ 20 % edge and corner blockages

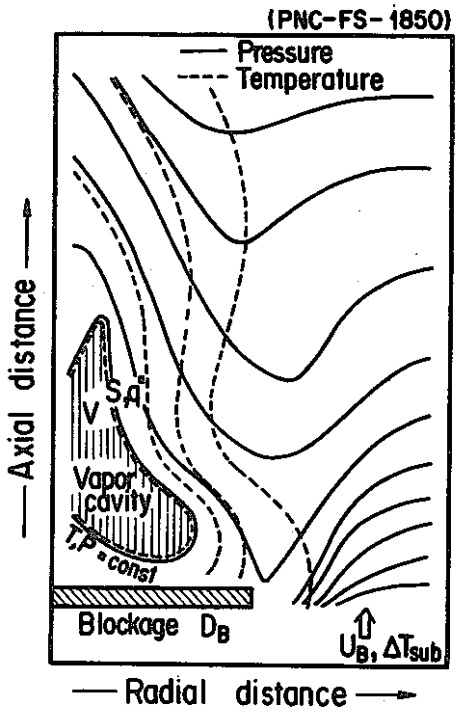

Fig. 12 Thermal and hydraulic boundary conditions for the vapor cavity stability

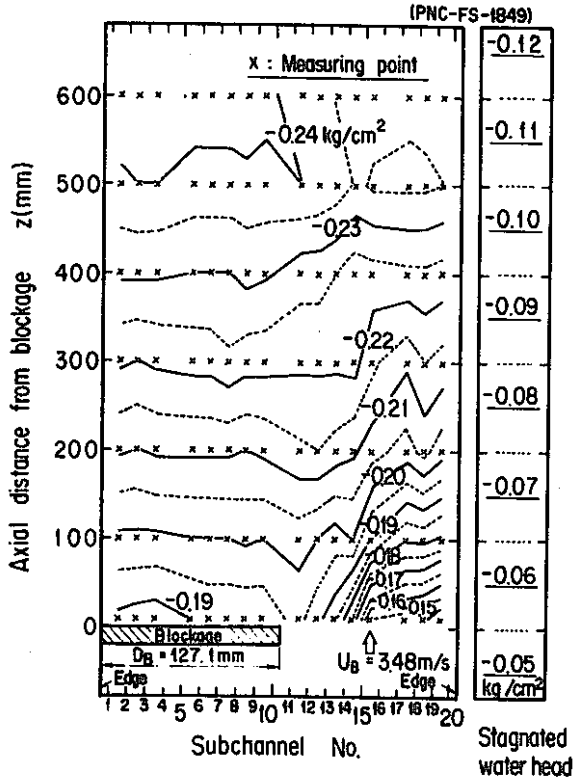

Fig. 13 Typical static pressure profile behind the 50 % edge blockage in a 61-pin bundle (water mockup single-phase flow test)

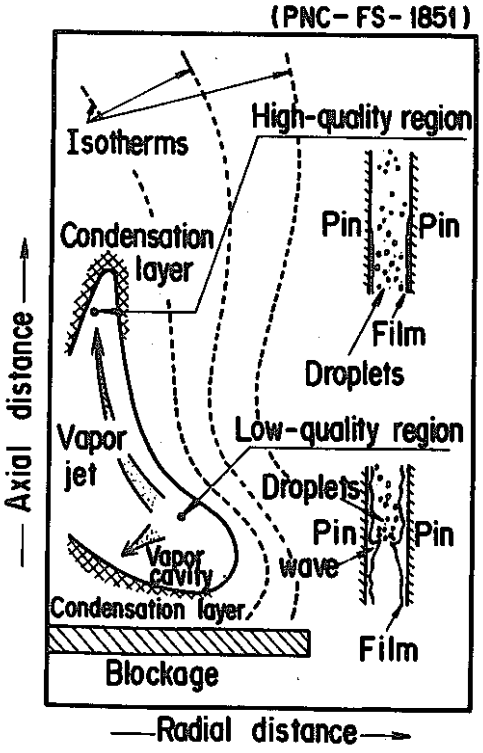

Fig. 14 Heat transport model within the vapor cavity